Wavelet-based texture segmentation of titanium based alloy lamellar microstructure: application to images from optical microscope and X-ray microtomography

L. Babout [1], Ł. Jopek [2], M. Janaszewski [1,2], M. Preuss [3], J.-Y. Buffière [4]

[1]*Computer Engineering Department, Technical University of Lodz, Poland lbabout@kis.p.lodz.pl*

[2] *The College of Computer Science, Lodz, Poland*

[3]*Materials Performance Centre, School of Materials, University of Manchester, UK*

[4]*MATEIS, INSA Lyon, France*

Reviewer: D. M. Scott (DuPont Company, USA)

Summary: A texture segmentation algorithm which combines grey level intensity from 2 images after discrete wavelet transform and variance has been applied on 2D images to segment lamellar colonies in (α+β) titanium alloy Ti6Al4V. Images were acquired using both optical microscope and X-ray tomography. The results are satisfying for the former technique and encouraging for the latter one. Possible extension of the method to volumetric data is presented.

Keywords: texture segmentation; Discrete Wavelet Transform; X-ray tomography; lamellar microstructure.

1. Introduction

Two-phases (α+β) titanium alloys are widely used in the aeronautical, power generation and biomedical industry because of excellent mechanical and corrosion properties combined with a relatively low density. The mechanical properties of these alloys, especially fatigue related properties are strongly dependent on variations in the microstructure. Most importantly, understanding the effects of microstructure on short crack growth behaviour of titanium alloys is critical. Recent work carried out at the ID-19 microtomography beamline at the European Synchrotron Radiation Facility (ESRF) has allowed to qualitatively correlate for the first time in 3D and in-situ the short crack propagation with the titanium fully lamellar microstructure, i.e. β-grain boundaries and orientation of α-lamellar colonies. (Babout et al., 2006).

A challenging computing task is then to automatically correlate the crack path with the microstructure. This correlation implies that the different phases, i.e. the crack, the β-grain boundaries and α-lamellar colonies are segmented separately. From an image processing point of view, the task to segment the different lamellar colonies is not conventional because an image of lamellar microstructure is a good example of textured image since it seems composed of repeated elements (the lamellae) with different interspacing and different orientations (a group of lamellae with the same orientation and relative constant interspacing forms a colony),. Moreover, classical segmentation methods based on intensity histogram cannot be used to segment and separate the different colonies. Even if the pattern in each α-lamellar colony does not repeat perfectly, image texture segmentation algorithms have been used for this work.

Texture is a commonly used feature in the analysis and interpretation of images. It is characterized by a set of local statistical properties of pixel intensities. It analyses the variations in the image, looking at properties such as smoothness, coarseness and regularity of patterns. Traditionally, texture features have been calculated using a variety of statistical, structural and spectral techniques including, co-occurrence matrices, spectral measures using filters such as Gabor filter (Teuner et al., 1995), fractal dimension and multi-resolution technique, such as wavelets (Mallat, 1989). The latter has been successfully used in image processing with the recent emergence of application to texture classification. The main advantages of the wavelet frames representation are that it focuses on scale and orientation texture features and it decomposes the image into orthogonal components.

This paper presents a first attempt to apply texture segmentation of lamellar titanium alloy microstructure. As a first step, the texture segmentation has been applied to 2D images from optical microscope and 2D reconstructed images from X-ray tomography of titanium alloy. The motivation of such preliminary test was to check the approach on 2D images, before the extension to 3D data. The manual inspection of the image has shown evidence that segmentation can be partly carried out based on quantitative description of directionality and grey level variation of the image texture. Directionality of lamellar colonies are extracted using discrete wavelet frames decomposition (Kim and Kang, 2007) and separation between colonies of the same directionality is performed using grey level variance. Firstly, the paper compares the result using standard optical microscope with segmented image using EBSD (Electron Back Scattered Diffraction microscope) technique. Secondly, it analyses the method applied on image from X-ray tomography. Limitations of the present method, other potential approaches possible and future works on extension to 3D case are finally proposed in the conclusion.

2. Images of the microstructure

The type of microstructure investigated in this paper, e.g. lamellar microstructure, appears in (α+β) titanium alloys during heat treatment, where β phase (bcc crystal lattice) transforms to α phase (hcp crystal lattice) during cooling of the sample. Description of the mechanism can be found in (Lutjering, 1998). A typical example of such microstructure, corresponding to titanium alloy

Ti6Al4V (90% Ti, 6% Alu, 4% V) and obtained using conventional optical microscope, is shown on Fig. 1, where β grain boundary and α-lamellae are visible: the α-lamellae, which can be schematised as lines are in dark, while the light grey background correspond to primary β-grains. Because the α-phase can develop within the β-phase with 6 possible variants (so called Burgers-relationship (Lutjering, 1998)), group of parallel-like lamellar, known as colonies, can have different orientations within the same β grain (see Fig. 1). It can also occur that colonies interpenetrate each other.

The same features from the same sample can also be observed in 2D longitudinal image reconstructed from X-ray tomography scans, as shown on Fig. 2. The corresponding set-up can be found in (Babout et al., 2006). The spatial resolution was set to 0.7 μm. In this figure, dark grey pixels correspond to β phase while white fringes, generated by phase contrast (Cloetens et al., 1997), indicate the presence of α-lamellae. The phase contrast is particularly crucial in this study case since it compensates the weak attenuation contrast between α and β phases. One can also notice that the image presents a higher level of noise than the one from optical microscope.

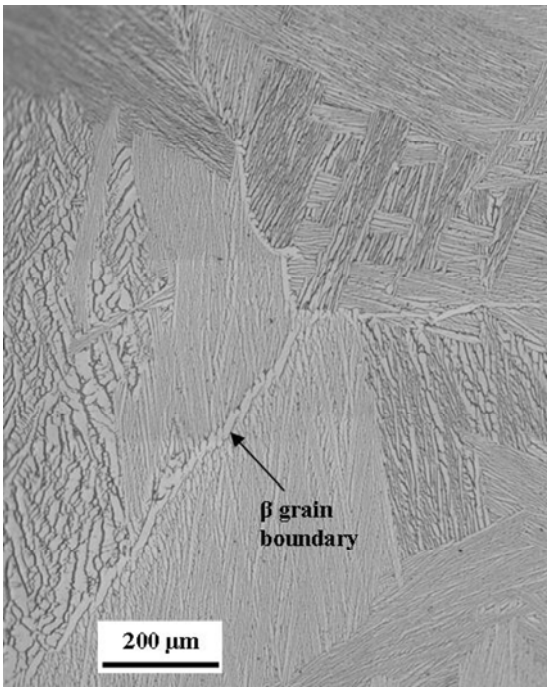

Fig. 1. Example of microstructure of fully lamellar titanium alloys obtained from optical microscope.

As mentioned above, lamellar colonies can be easily separated by eye, due to their preferential directionality. One can also notice that the variation of thickness of the lamellae and their interspacing within different colonies give rise to changes in local grey level contrast, especially in Fig. 1, hence facilitating the separation between colonies. These two features, directionality and local variance in contrast are common properties used in texture segmentation. The following section describes how they are used to segment the colonies.

3. Texture segmentation method

The method considered different sets of images for the texture segmentation: the original image and so-called detail images after Discrete Wavelet Transform decomposition (DWT) of the original one. Wavelets have been shown to be useful for texture analysis, possibly due to their finite duration, which provides both frequency and spatial locality. The hierarchical wavelet transform uses family of wavelet functions and its associated scaling functions to decompose the original image/signal into different sub-bands (Mallat, 1989). Example of such decomposition at level 1 is shown on Fig. 3. The decomposition has been obtained using MaZda, a texture analysis software (Strzelecki et al., 2006). The figure shows the so-called Approximation Image (*A1*; top-left), the Vertical Detail Image (*V1*; bottom-left), the Horizontal Detail Image (*H1*; top-right) and the Diagonal Detail Image (*D1*; bottom-right). The Details images have been binarised and inverted to enhance the contrast between colonies of different directionality. These images are obtained from the decomposition of the original image using combination of low-pass and high-pass bands based on Haar wavelet (Dettori and Semler, 2007), along x- and y- directions of the input image. For instance, *H1* is obtained from the original one by consecutively convolving the image with the low-pass filter along x-direction and the high-pass filter along y-direction. During decomposition, approximation and detail images are down-sampled, resulting in images 4 times smaller than the original image. In order to create decomposed images of the same size as the original one, the input image is then up-sampled prior to wavelet decomposition. The Approximation Image at level 1 can as well be decomposed into 4 sub-images, and the process can be repeated recursively up to a filtered images of size 1 (pixel). The wavelet decomposition is then a multi-resolution technique since at each level of decomposition the spatial resolution is decreased by a factor of 2.

One can see from Fig. 3 that *V1* and *H1* exhibit higher contrast than in the original image for colonies which tend to be perpendicular and parallel to x-direction, respectively. On the other hand, *D1* does not exhibit such trend. Therefore, *H1* and *V1* are used preferentially for the following step of the texture segmentation method. It consists in generating a new image A*1* for which each pixel is classified as follows:

$$p_{A1,xy} = \begin{cases} 0 & I(V1_{xy}) > I(H1_{xy}) \\ & + \delta \min\left(I(V1_{xy}), I(H1_{xy})\right), \\ 127 & I(V1_{xy}) < I(H1_{xy}) \\ & + \delta \min\left(I(V1_{xy}), I(H1_{xy})\right), \\ 255 & \left|\dfrac{I(V1_{xy}) - I(H1_{xy})}{\min\left(I(V1_{xy}), I(H1_{xy})\right)}\right| \le \delta \end{cases} \quad (1)$$

Where $p_{A1,xy}$ is the grey level of the pixel at coordinate *(x,y)*, δ an empirical dimensionless factor smaller than 0.1, $I(V1_{xy})$ and $I(H1_{xy})$ are local mean grey

level intensities, as described by the following general expression:

$$I(A_{xy}) = \frac{1}{(2r+1)^2} \sum_{i=x-r}^{x+r} \sum_{j=y-r}^{y+r} p_A(i,j) \quad (2)$$

where A is a given analysed image, $2r+1$ the size of the analysing window and $p_A(i,j)$ the grey level of the pixel at coordinate (i,j). The third classifier in equation 1 ($p_{A1,xy}=255$) corresponds to the situation where there is no preferential directionality (either vertical or horizontal) at the current position. In practice, δ is selected after comparison of the data in ROIs where both $H1$ and $V1$ present similar grey level intensity.

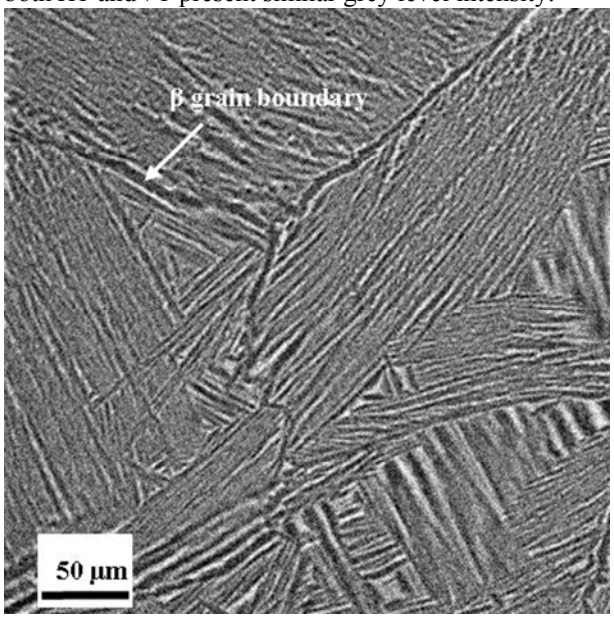

Fig. 2. 2D reconstructed longitudinal image from X-ray tomography scan of the same type of fully lamellar microstructure shown in Fig. 1.

The second step of the texture segmentation is based on local analysis of the grey level variance parameter in the original image. The variance σ^2 is one of texture measures that can be used to discriminate among different texture pattern classes. This parameter tells about how spread out the distribution of grey level is. For a window (also called ROI) of size NxM centred at pixel position (x,y) the variance calculated for an image A is given by:

$$\sigma^2 \equiv \sigma^2(A_{xy}) = \sum_{i=1}^{N_g} (i - I(A_{xy}))^2 h_A(i) \quad (3)$$

where N_g denotes the number of intensity levels (i.e. 256 in the present case), $h(i)$ is a normalized histogram vector (i.e. histogram whose entries are divided by the total number of pixels in ROI) and $I(A_{xy})$ is the mean intensity defined by equation 2.

A new set of classifier is defined depending on the value of the variance. The range of variance value of the image is separated into 3 regions delimited by:

$$P_1 = C_1 + \varepsilon$$
$$P_2 = C_2 - \varepsilon \quad (4)$$

Where $C1$ and $C2$ are the minimum and maximum variance of all windows extracted from the input image, respectively and ε a scale factor defined by:

$$\varepsilon = (C_2 - C_1) \times \delta' \quad (5)$$

Where δ' is an empirical factor with value ranging between 0.1 and 0.5. A new image $A2$ is created based on the following class of pixels, depending on their variance value (low, middle and high):

$$p_{A2,xy} = \begin{cases} 0 & \sigma^2 < P_1, \\ 127 & \sigma^2 < P_2 \wedge \sigma^2 \geq P_1, \\ 255 & \sigma^2 > P_2 \end{cases} \quad (6)$$

Finally, the pixels of the final image A_{fs} are classified into 7 different classes $cl_{1\to7}$ based on their corresponding value in $A1$ and $A2$:

$$cl_1 = \{(x,y) \in Z^2 ; p_{A1,xy} = 0 \wedge p_{A2,xy} = 0\}$$
$$cl_2 = \{(x,y) \in Z^2 ; p_{A1,xy} = 0 \wedge p_{A2,xy} = 127\}$$
$$cl_3 = \{(x,y) \in Z^2 ; p_{A1,xy} = 0 \wedge p_{A2,xy} = 255\}$$
$$cl_4 = \{(x,y) \in Z^2 ; p_{A1,xy} = 127 \wedge p_{A2,xy} = 0\} \quad (7)$$
$$cl_5 = \{(x,y) \in Z^2 ; p_{A1,xy} = 127 \wedge p_{A2,xy} = 127\}$$
$$cl_6 = \{(x,y) \in Z^2 ; p_{A1,xy} = 127 \wedge p_{A2,xy} = 255\}$$
$$cl_7 = \{(x,y) \in Z^2 ; p_{Acl1}(x,y) = 255\}$$

The definition of the class 7 is not taking into account the variance since the areas around the pixels of this class do not exhibit directionality, hence variation in the average intensity.

Values assigned to pixels from classes 1 to 7 were set to 0, 75, 125, 150, 175, 200 and 255, respectively. It is worth mentioning that the method described above has not been thought to assess or not the possibility of using wavelet-based texture segmentation method to the microstructure of interest. The following scenario has then been thought: testing the approach on a 2D model "little-noise" image of lamellar microstructure where good texture segmentation is expected and on 2D "real" image of the same microstructure obtained using X-ray tomography to analyse the possible limitations of the method and foresee new strategies.

4. Application to 2D images from Optical Microscope

Fig. 4 displays the result of the above method to the image presented in Fig. 1. Particularly, it shows the pixel classification after the wavelet transform (Fig. 4b), and the final segmented image (Fig. 4c). The size of the

original image is 1070 pixels in width and 1250 pixels in height. The features (mean intensity in decomposed images and variance) were calculated for each pixel of the original image using a local window of size 25x25 centred on the corresponding pixel. The problem encountered for the pixels nearer to the edge of the image than the half-width of the window, is solved by assuming that the image edges are mirrors, so that each row or column containing these pixels is duplicated beyond it. The window size of 25x25 was found a good compromise between the reliability of the calculated texture features and the accuracy of boundary localisation in texture segmentation. Moreover, the choice of δ and δ' set to 0.1 and 0.2 (equations 1 and 5) was found to provide the best texture segmentation. The corresponding variance boundaries, P1 and P2 defined in equation 4, were set to 700 and 2820, based on the minimum and maximum variance of all windows extracted from the image, i.e. 0 and 3520, respectively.

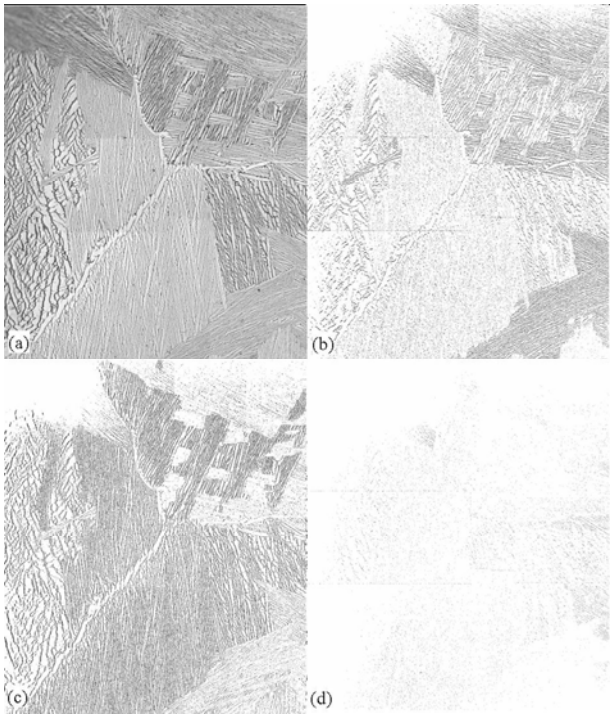

Fig. 3. Wavelet transforms applied to image shown in Fig. 1. (a) Approximation image, (b), Horizontal Detail image, (c), Vertical Detail image and (d) Diagonal Detail image.

One can notice that the first classification based on the local intensity of wavelet transform decomposition separates relatively well colonies with nearly-horizontal and vertical orientations. Only few boundary between areas with strong horizontal details and vertical details present no preferential directionality (very thin white layers and spots in Fig. 4b). The final segmentation compares also relatively well with an EBSD[1] map of the same region (**Error! Reference source not found.**d), showing the relative good effect of variance classification to separate colonies of the same wavelet-based classification. It is worth noticing that even 7 classes of features properties were defined in equation 7, the colonies are mainly classified as cl_1, cl_2, cl_4 and cl_5, as shown in Fig. 4c. Mean variance and corresponding standard deviation of the 11 colonies indexed in Fig. 4a are listed in Table 1. The values have been calculated over 10 windows of size 25x25 manually selected in each colonies. The results show particularly good boundary discrimination between colonies 7 and 8, where mean variances are different and standard deviation low (small fluctuation of the variance indicating regularity of the lamellar pattern in these colonies). However, the texture segmentation fails to separate features where the mean variance is of similar order of magnitude, for instance, between colonies 5 and 7 (~520 in both zones) or 9 and 10. In the former case, the method shows as well its current limitation to detect the grain boundary, present between these 2 colonies. Finally, the variance shows some limitation to accurately discriminate boundary of colonies where interspacing between lamellae is irregular and of the length as the size of the analyzing window, illustrated by large fluctuation of the variance value, such as in zone 4.

Table 1. Mean and standard deviation of variance in 11 zones (colonies) indexed in Fig. 4a. Values have to be multiplied by 1E+3.

zone	1	2	3	4	5	6
mean	0.18	0.28	1.15	0.99	0.52	0.60
Std	0.12	0.12	0.17	0.36	0.11	0.09
zone	7	8	9	10	11	
mean	0.52	0.80	0.29	0.40	0.15	
std	0.16	0.17	0.06	0.07	0.04	

5. Application to reconstructed images from X-ray tomography

The method presented in the previous section was in the case of the best scenario where features of the image with different orientations and grey level intensities are clearly distinguishable. The type of image, presented in this section, is of greater importance since it is directly linked to the main goal of correlating in 3D using X-ray tomography the propagation of a crack with the microstructure of lamellar titanium alloy. However, such images contain a higher level of noise than in the previous case, reducing the perception of lamellar colonies. Not only noise but also weak phase contrast resulting of unresolved lamellar at the given spatial resolution of the system (in the present case, 0.7 μm) may also weaken locally the colony segmentation. Therefore, the method has been applied to 2D reconstructed images of the same material observed using optical microscope, i.e. Ti64 sample, before considering the 3D case.

[1] EBSD is a microscopy technique which scans regions of a sample to determine crystal lattice orientation maps based on the diffraction of an X-ray beam with the sample under investigation.

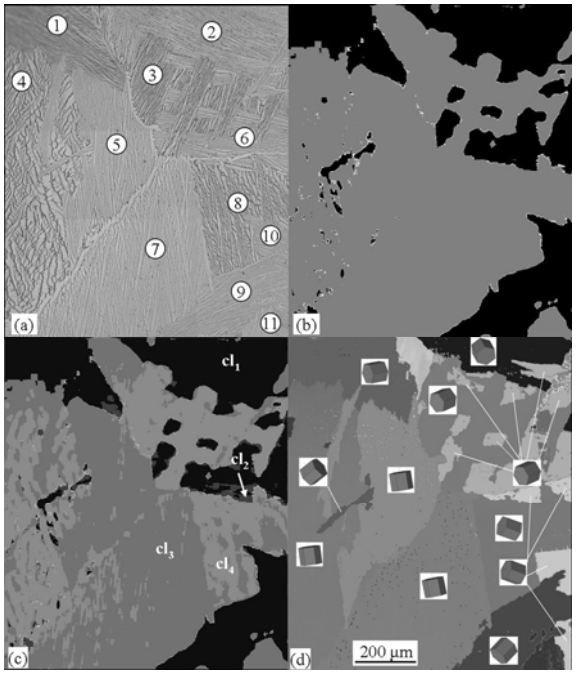

Fig. 4. (a)Image from optical microscope and corresponding segmented results: (b) segmentation after wavelet classification (c) final segmentation (d) EBSD map of the same region as (a) showing the different hcp crystal lattice orientation of the colonies.

Fig. 5 displays the result of the texture segmentation of the reconstructed image shown in Fig. 2 (500x500 pixels). The features (intensity in decomposed images and variance) at pixel (x,y) were calculated within a local window of size 32x32 centred on the corresponding pixel. This window was set larger than the window in the previous example because of higher level of noise in the image. Moreover, the choice of δ and δ' were set to 0.1 and 0.4, the latter showing, for the author's point of view, the best texture segmentation. The pixels in this image present a variance between 840 and 4790, which result in variance boundaries P1 and P2 equal to 2620 and 3015, respectively.

In general, the result of the texture segmentation shown in Fig. 5c, superimposed on the original image as shown on Fig. 5d, is less satisfying than in the previous case, i.e. image from the optical microscope. However, due to the complexity of the image, results are encouraging. Indeed, one can notice than some boundary discriminations between colonies are relatively accurate, such as between colonies 1 and 2, 1 and 5 or 5 and 6, which, in these cases, are mainly due to rather good wavelet decomposition (see Fig. 5b). Some small regions, such as zones 3 and 4 are also detected. However, the decomposition fails, like in the previous example, to delimitate colonies of the same orientation separated by a grain boundary, such as colony 1 and the one which stands above colony 3 in Fig. 5a. As expected, areas which correspond to the third class from wavelet decomposition (equation 1), i.e. without preferential directionality (white colour), occur at boundaries between colonies with strong misorientation. Two large white areas can also be noticed between zones 2 and 3, 3 and 5. While the former area results from misorientation of colonies within the same grain, the latter one surprisingly corresponds to a portion of zone 5. The possible reason which could explain the presence of no preferential directionality in this zone is the average orientation of the lamellae at 45° which may result, after wavelet decomposition, to nearly equal local intensity in the corresponding Horizontal and Vertical Detail images. Finally, the boundary discrimination is not satisfying in zones where the lamellar directionality is fading, such as in zone 7. However, Fig. 6 shows that the lamellae are better distinguishable and regularly spaced in another orthogonal plane. The boundary discrimination may therefore be more accurate in this plane for this colony.

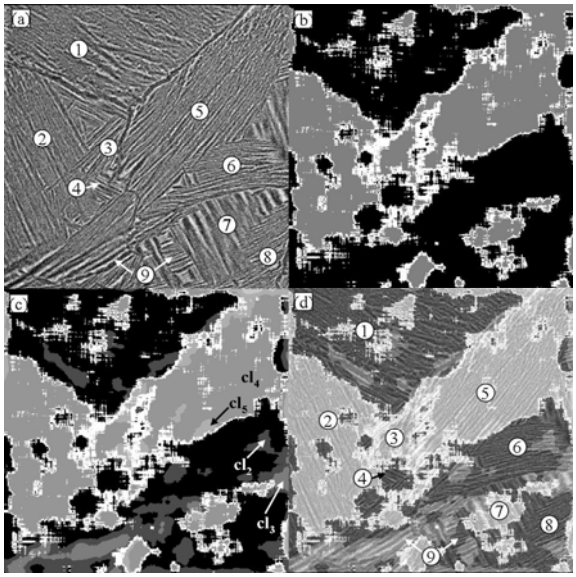

Fig. 5. (a) image from X-ray tomography and corresponding segmented results (b) segmentation after wavelet classification (c) final segmentation (d) superposition of (a) and (c).

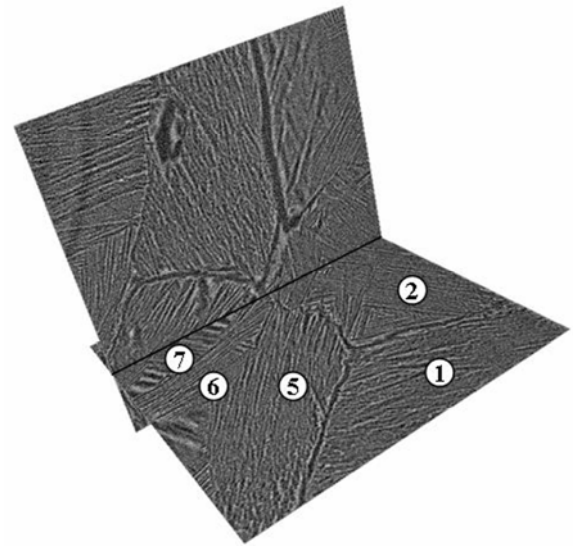

Fig. 6: 3D view showing the reconstructed image of Fig. 5a with another orthogonal plane crossing the colonies 2 and 5.

The superposing effect of variance for the pixel classification is less significant and precise than in the previous example to accurately separate colonies of the same wavelet classification. However, the algorithm is relatively able to distinguish them, as it can be seen on Fig. 5c and Fig. 5d where colonies 6 and 8 are relatively well detected. Colony 9 presents large variance fluctuation, as shown in Table 2, which explains partly why the zone contains areas of class cl_1, cl_2 and cl_3 (see equation 7).

Table 2 Mean and standard deviation of variance in 7 zones (colonies) indexed in Fig. 5a. Values have to be multiplied by 1E+3.

zone	1	2	3	5	6	7	9
mean	1.66	1.34	2.4	1.82	1.85	2.07	3.30
std	0.47	0.21	0.20	0.28	0.35	0.65	0.63

6. Discussion and conclusion

This paper has presented a preliminary approach based on wavelet-based texture segmentation method to segment lamellar colonies in (α+β) titanium alloy. The primary aim of the paper was not to present an optimised method but rather to show its applicability and limitations to the present study. Segmentation results of images of the same titanium-based microstructure from optical microscope and X-ray tomography have shown that this method, which does not take into account any prior knowledge of the texture pattern, works relatively well when the lamellae are clearly distinguishable and the pattern in colonies regular. However, the present method does not detect grain boundaries which may be of importance when it separates two colonies of the same orientation. This is a crucial point in the future study of correlation between crack path and microstructure since it is known that grain boundaries in lamellar titanium alloys deflect cracks. A possible method would be to specify a special class of grey level features which discriminate only grain boundaries among all the patterns which compose the lamellar image. Moreover, the choice of the boundaries for the variance classification may also be problematic to adequately discriminate connected colonies of the same orientation. The present method was simply considering 3 ranges of variance value, based on the minimum and the maximum variance of the image, while another approach could consider a study of the variance histogram to select the ranges. Before considering the extension to 3D data, other approaches could be tested, like co-occurrence matrices (Haralick and Shapiro, 1992) and ridgelet transform (Donoho, 2001). Grey Level Co-occurrence Matrices method (GLCM), which is defined over an image to be the distribution of co-occurring values at a given offset, is often used in texture analysis since it is able to capture the spatial dependence of gray-level values within an image. The method is sensitive to rotation and particularly sensitive to regular patterns, and may therefore be of utility to analyse lamellar structure. A possible approach would be to pre-define window samples, extracted directly from the analysed image, or generated automatically to resemble to different lamellar patterns, and compare the properties of the corresponding GLCM with the ones of the image. However, this method would have a high time complexity. Ridgelet transform is a recent multi-resolution analysis tool based on Wavelet transform, which capture structural information of an image based on multiple radial directions in the frequency domain (Donoho, 2001). The image decomposition considers more than 3 detail images as for DWT (vertical, horizontal and diagonal), and may therefore be of better interest to discriminate adjacent lamellar colonies with opposite orientations. These new approaches are currently under development and testing. The best method will then be extended for 3D texture analysis. Two main strategies will be evaluated: treating 3D data as a stack of 2D images in the 3 principal directions and defining real volumetric texture analysis. The former method has already been used to denoise volumetric data of breast using 3D wavelet transforms (Chen and Ning, 2004)

Acknowledgments

The authors would like to thank Dr J. Bennett of the School of Materials, University of Manchester, who scanned the titanium sample using the X-ray tomography setup of the ID19 beam line at the ESRF.

REFERENCES

BABOUT L., MARROW T.J., PREUSS M., (2006), Sequential X-ray Tomography Studies of Damage Assessment in Materials Science, 4th Symposium on Process Tomography in Poland, Warsaw, pp. 159-162.

CHEN Z., NING R., (2004), Breast volume denoising and noise characterization by 3D wavelet transform, *Computerized Medical Imaging and Graphics*, Vol. 28, pp. 235-246.

CLOETENS P., PATEYRON-SALOME M., BUFFIERE J.Y., PEIX G., BARUCHEL J., PEYRIN F., SCHLENKER M., (1997), Observation of microstructure and damage in materials by phase sensitive radiography and tomography, *Journal of Applied Physics*, Vol. 81, pp. 5878-5886.

DETTORI L., SEMLER L., (2007), A comparison of wavelet, ridgelet, and curvelet-based texture classification algorithms in computed tomography, *Computers in Biology and Medicine*, Vol. 37, pp. 486-498.

DONOHO D., (2001), Ridge functions and orthonormal ridgelets, *Journal of Approximation Theory*, Vol. 111, pp. 143-179.

HARALICK R.M., SHAPIRO L.G., (1992), *Computer and robot vision*, Addison-Wesley Publishing Co., Boston, p. 630.

KIM S.C., KANG T.J., (2007), Texture classification and segmentation using wavelet packet frame and Gaussian mixture model, *Pattern Recognition*, Vol. 40, pp. 1207-1221.

MALLAT S.G., (1989), A theory for multiresolution signal decomposition: the wavelet representation, *IEEE*

Transactions on Pattern Analysis and Machine Intelligence, Vol. 11, pp. 674-693.

STRZELECKI M., MATERKA A., SZCZYPINSKI P., (2006), *MaZda*. Texture Analysis for Magnetic Resonance Imaging, Med4publishing, Prague. pp. 105-111.

TEUNER A., PICHLER O., HOSTICKA B.J., (1995), Unsupervised texture segmentation of images using tuned matched Gabor filters, *Image Processing, IEEE Transactions on*, Vol. 4, pp. 863-870.